Quantum Yield for O(^{1}D) Production from Ozone Photolysis in the Wavelength Range of 193−225 nm

Satoshi Nishida, Fumikazu Taketani, Kenshi Takahashi,* and Yutaka Matsumi

Solar-Terrestrial Environment Laboratory and Graduate School of Science, Nagoya University, Honohara 3-13, Toyokawa, Aichi, 442-8507, Japan

Received: January 1, 2004; In Final Form: February 4, 2004

The quantum yield values for O(^{1}D) production from the photodissociation reaction of O_3 between 193 and 225 nm at 298 ± 2 K are reported. The O(^{1}D) photofragments have been detected directly using a technique of vacuum ultraviolet laser-induced fluorescence spectroscopy at 115.22 nm which is associated with the electronic transition of O($3s^1D^\circ - 2p^1D$). It has been found that the O(^{1}D) quantum yield values decrease monotonically as the photolysis wavelength becomes shorter from 0.90 ± 0.12 (225 nm) to 0.48 ± 0.03 (193 nm). Photodissociation processes of O_3 around 210 nm and its atmospheric implications have been discussed.

Introduction

Photodissociation reaction of O_3 in the ultraviolet (UV) region has been extensively studied due to its pivotal role in the Earth's atmosphere and the fundamental interest on the photochemical properties of the simple polyatomic molecules.[1,2] The UV photoabsorption spectrum of O_3 shows a broad feature with a maximum around 255 nm ($\sigma_{O3} = 1.1 \times 10^{-17}$ cm^2 molecule^{-1}),[3−5] and the strong absorption band between 205 and 310 nm is called a Hartley band. The photodissociation reaction in the Hartley band gives rise to two different pathways mainly:

$$O_3 + h\nu \rightarrow O(^3P) + O_2(X^3\Sigma_g^-) \quad (1)$$

$$O_3 + h\nu \rightarrow O(^1D) + O_2(a^1\Delta_g) \quad (2)$$

At the blue side of the Hartley band, the photoabsorption cross sections show a minimum around 201 nm (3.1×10^{-19} cm^2 molecule^{-1})[4] and increase again as the wavelength becomes shorter, indicating that a new absorption band starts. For instance at 193 nm, 10 different dissociation pathways after photoexcitation are thermochemically available as listed in Table 1.[6] Among the photoproducts, the chemical reactions of O(^{1}D) atoms with small atmospheric molecules are quite important for understanding the photochemical processes of the Earth's atmosphere. Therefore, there have been several reports on the experimental determinations of the quantum yield for O(^{1}D) production in the UV photolysis of O_3 between 221 and 330 nm.[1,2,7−9] Those experimental studies showed that the O(^{1}D) quantum yields between 230 and 300 nm are almost independent of the photolysis wavelength with an average value of 0.91,[9] while those above 300 nm decrease drastically as the photolysis wavelength becomes longer, ranging from 0.91 to 0.08.[1,2,7] Turnipseed et al.[10] measured the O(^{1}D) quantum yield from O_3 photolysis at 222 nm to be 0.87 ± 0.04, which is close to the average O(^{1}D) quantum yield value of 0.91 between 230 and 300 nm. They also reported the O(^{1}D) and O(^{3}P) quantum yields at 193 nm to be 0.46 ± 0.29 and 0.57 ± 0.14, respectively, by means of a technique of resonance fluorescence using an oxygen atom resonance lamp. Stranges et al.[11] photolyzed the O_3 molecular beam and studied the multiple-channel dissociation dynamics using a technique of photofragment translational spectroscopy. They estimated that the branchings for channels of O(^{3}P) + O_2(X), O(^{3}P) + O_2(X, vibrationally hot), O(^{1}D) + $O_2(a^1\Delta_g)$, O(^{1}D) + $O_2(b^1\Sigma_g^-)$, and 3O(^{3}P) to be 16.8, 7.7, 45.5, 23.3, and 2.0%, respectively, and the rest of the branchings was not definitely assigned. Very recently, Takahashi et al.[12] detected the O(^{1}S) atoms from the 193-nm photodissociation of O_3 using a technique of vacuum UV laser-induced (VUV-LIF) fluorescence at 121.76 nm and determined its quantum yield of 2.5 (±1.1) × 10^{-3}. The quite small quantum yield value for O(^{1}S) formation indicates that O(^{1}D) and O(^{3}P) are dominant photoproducts in the photolysis of O_3 at 193 nm. Cooper et al.[13] detected the O(^{1}D) atoms from the photodissociation of O_3 between 221 and 243.5 nm by observing the weak fluorescence at 630 nm which is associated with the spin-forbidden $^1D_2-^3P$ transition. The reported O(^{1}D) quantum yield values lay in the range 0.87−0.88. At wavelengths between 193 and 221 nm, however, there has been no report on measurements of the quantum yield values of O(^{1}D) production from O_3 photolysis.

TABLE 1: Thermochemical Threshold Wavelengths (nm) for Photodissociation Pathways of O_3

	$O_2(X^3\Sigma_g^-)$	$O_2(a^1\Delta_g)$	$O_2(b^1\Sigma_g^+)$	$O_2(A^3\Sigma_u^+)$	$O_2(B^3\Sigma_u^-)$	$2O(^3P)$
O(^{3}P)	1180	590	460	230	170	198
O(^{1}D)	410	310	260	167	150	
O(^{1}S)	234	196	179	129	108	

In this paper, we report the experimental measurements of the O(^{1}D) quantum yields from the photodissociation of O_3 at 225, 220, 215, 210, 206, and 193 nm. The O(^{1}D) photofragments were detected directly using VUV-LIF spectroscopic techniques and the relative LIF signal intensities were calibrated to determine the O(^{1}D) quantum yield by two methods as described below. All the experiments were performed at 298 ± 2 K. Photodissociation processes of O_3 in the deep-UV region around 210 nm have been discussed based on the O(^{1}D) quantum yields obtained in this work. Implications of the present results for stratospheric ozone chemistry are also discussed.

* Corresponding author. E-mail: kent@stelab.nagoya-u.ac.jp. Fax: +81-533-89-5593.

10.1021/jp049979r CCC: $27.50
Published on Web 03/17/2004

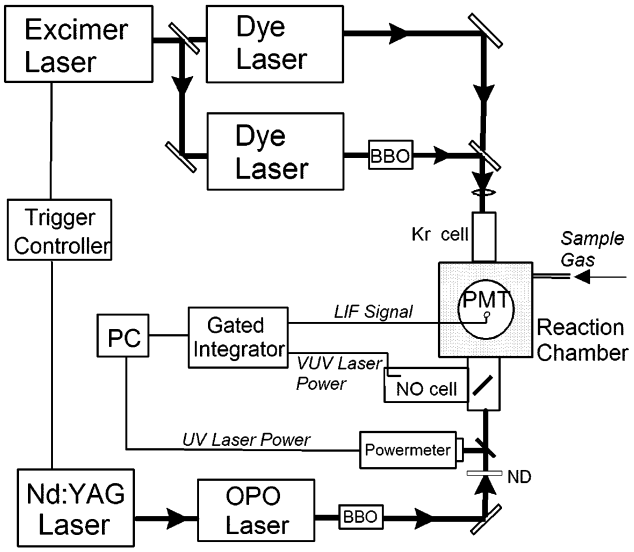

Figure 1. Schematic diagram of the experimental setup used in this study, depicting the system to measure the O(1D) quantum yields from ozone photolysis at 206−225 nm. For measurements of the O(1D) quantum yield at 193 nm, an Excimer laser was used instead of the tunable photolysis light source of an OPO laser that was pumped by a Nd: YAG laser (see text). The excimer laser is not depicted in this Figure. PM: power meter, ND: neutral density optical filter, BBO: β-BaB_2O_4 crystal, and PC: personal computer.

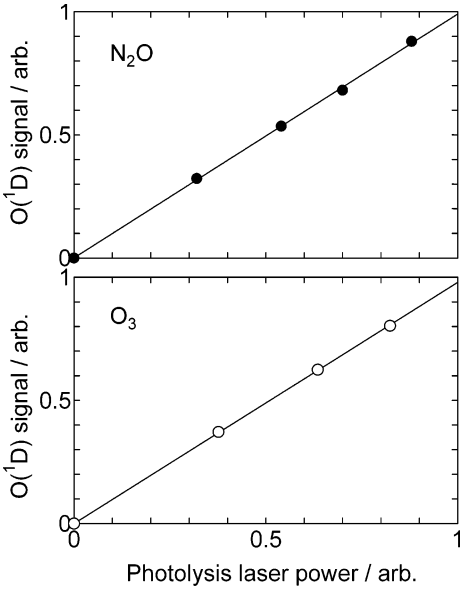

Figure 2. Photolysis laser power dependence of the signal intensity of O(1D) from the 193 nm photolysis of N_2O (upper panel) and O_3 (lower panel) under the same experimental conditions that the O(1D) quantum yield was measured. The O(1D) atoms were detected by laser-induced fluorescence (LIF) at 115.22 nm which is associated with the O($3s^1D^\circ - 2p^1D$)) transition. Straight lines indicate the results of linear least-squares fit analysis.

Experimental Section

The experimental setup used in this study was almost same as that in our previous studies about O_3 photochemistry.[9,12,14] Figure 1 shows a schematic diagram of the experimental setup which was used in the present study. All of the experiments were performed at 298 ± 2 K. The O(1D) photofragments produced in the UV photolysis of O_3 were detected directly by using a VUV-LIF technique. The probe laser beams for the O($3s^1D^\circ-2p^1D$) transition at 115.22 nm were generated by the phase-matched frequency tripling in the Xe/Ar mixture.[15] The UV laser around 345.6 nm from an XeCl excimer laser pumped dye laser (Lambda Physik, COMPex 201 and FL3002E) was focused into a cell containing a Xe/Ar mixture (10 Torr/200 Torr). Typical pulse energy of the UV laser was 6 mJ. The VUV photons at 115 nm were introduced into a reaction chamber through a LiF window that separated the Xe/Ar cell and the reaction chamber. A part of the generated VUV photons was reflected into a photoionization cell containing 2 Torr of nitric oxide (NO) by a thin LiF plate. By monitoring the photoionization current from the NO cell, relative intensity variations of the VUV laser were measured.

The photolysis laser beam which was tunable between 206 and 230 nm was obtained by frequency doubling of the signal light from an Nd:YAG pumped optical parametric oscillator (OPO) laser (Continuum, Powerlite 8010 and Panther OPO) in a β-BaB_2O_4 (BBO) crystal. Dichloic mirrors were used to separate the fundamental and UV outputs. The bandwidth of the UV radiation was ~6 cm^{-1} (fwhm). The wavelength calibration of the OPO signal light was achieved simultaneously with measurements of the O(1D) spectra by introducing a part of the OPO signal light into a wavemeter (Coherent, Wavemaster). Typical pulse energy of the UV photolysis radiation was 0.4−1 mJ. During the experiments, the UV laser power was monitored on a shot-by-shot basis using a pyroelectric laser power meter (Molectron, J4−09). A part of the UV photolysis laser was reflected by a thin fused silica plate onto the power meter. We also monitored the photolysis laser power with a calorimeter (Scientech, AC50UV) by inserting its detector head into the photolysis laser beam path in front of the reaction cell after every LIF measurement. An excimer laser operated with an ArF mode was also used as a photolysis radiation at 193 nm (Lambda Physik, COMPex 102) instead of the OPO laser. The excimer laser is not depicted in Figure 1.

The time delay between the photolysis and probe laser pulses was controlled by a pulse generator (Stanford Research, DG535), which was typically set to be 100 ns. The LIF signal was detected along the vertical direction, orthogonal to the propagation direction of both the photolysis and probe laser beams, by a solar-blind photomultiplier tube (EMR, 541J-08-17). The fluorescence detection direction was parallel to the electric vector of the photolysis laser and perpendicular to that of the probe laser. This photomultiplier tube was equipped with a LiF window and a KBr photocathode and has its sensitivity only in the wavelength range of 106−150 nm. The output from the photomultiplier was accumulated using a gated integrator (Stanford Research, SR-250) over 10 shots of photolysis laser pulses and stored on a personal computer.

The O_3 gas was produced by passing ultrapure O_2 (Nagoya Kosan, 99.9995%) through an ozonizer. The reaction chamber was evacuated by a rotary pump and a mixture of O_3/He was slowly fed into the chamber through the poly(tetrafluoroethylene) needle valve. The total pressure in the chamber was maintained to be 1.0 Torr and the partial pressure of O_3 was about 3 mTorr. The total pressure was measured with a capacitance manometer (MKS, Baratoron 220) during the experiments. The partial pressure of O_3 in the chamber was monitored by absorption spectrometry at 253.7 nm using a low-pressure mercury pen ray lamp. It should be noted that the high sensitivity of the VUV-LIF technique allows detection of O(1D) atoms at such low pressures and at short pump−probe delay times and that secondary reactions of O(1D) can be ignored. For example, the rate constant for O(1D) + O_2 reaction was reported to be 4.0×10^{-11} cm^3 $molecule^{-1}$ s^{-1} at 298 K,[8] which was so slow that it could not interfere with the measurements

under our experimental conditions. Helium used as a buffer gas was an inefficient quencher for $O(^1D)$.[16]

We checked the photolysis laser power dependence of the LIF signal of $O(^1D)$ atoms, and the typical results are shown in Figure 2. Figure 2 shows the plots of the LIF intensities of $O(^1D)$ produced from the photodissociation of O_3 and N_2O at 193 nm as a function of the 193-nm laser power. It was found that the $O(^1D)$ LIF signal intensity was linearly dependent on the photolysis laser at all photolysis wavelengths studied here under our experimental conditions. Furthermore, no LIF signal of $O(^1D)$ was observed when the photolysis laser was turned off. These results indicate that both the multiphoton absorption of O_3 to produce $O(^1D)$ and the photodissociation reaction of O_3 around 115.22 nm could safely be ignored under our experimental conditions.

Results and Discussions

Since the LIF measurements provide only relative concentrations of the species detected, the calibration of the LIF intensities is needed to obtain their absolute quantum yield values. In our present study, two different ways of the LIF intensity calibration were performed to determine the absolute quantum yield values of $O(^1D)$ production from O_3 photolysis in the UV region. For the $O(^1D)$ quantum yield determination at 193 nm, photodissociation reaction of N_2O at 193 nm to produced $O(^1D)$ was utilized as a reference:

$$N_2O + h\nu\ (193\ \text{nm}) \rightarrow O(^1D) + N_2 \qquad (3)$$

The known concentrations of N_2O molecules and O_3 molecules were photolyzed alternatively at 193 nm, and the LIF signal intensities of $O(^1D)$ produced photolytically were directly detected by the VUV-LIF technique. The probe laser wavelength was scanned over the $O(3s^1D^\circ - 2p^1D)$ transition, which was broadened because of partitioning of the available energy. By comparing the peak area of the fluorescence excitation spectra of $O(^1D)$, $S_{O3}(193)$ and $S_{N2O}(193)$, from the photodissociation of O_3 and N_2O at 193 nm, the quantum yield for $O(^1D)$ production from O_3 photolysis at 193 nm, $\Phi^{1D}{}_{O3}(193)$, could be derived using the following expression,

$$\Phi^{1D}{}_{O3}(193) = \frac{S_{O3}(193) \times \sigma_{N2O}(193) \times [N_2O] \times \Phi^{1D}{}_{N2O}}{S_{N2O}(193) \times \sigma_{O3}(193) \times [O_3]} \qquad (4)$$

in which $[N_2O]$ and $[O_3]$ indicate the number density of those molecules in the chamber, and $\sigma_{O3}(193)$ and $\sigma_{N2O}(193)$ are the room-temperature absorption cross sections of O_3 (4.28×10^{-19} cm^2 molecule^{-1})[8] and N_2O (8.95×10^{-20} cm^2 molecule^{-1})[8] at 193 nm. The quantum yield for $O(^1D)$ production in reaction 3, $\Phi^{1D}{}_{N2O}$, is very close to unity ($\Phi^{1D}{}_{N2O} \approx 1$), because other processes are minor.[8,17,18]

For determination of the quantum yields for $O(^1D)$ formation from O_3 photolysis at 206, 210, 215, 220, and 225 nm, the ratios of the $O(^1D)$ LIF intensities at those photolysis wavelengths relative to those at 230 nm were measured. Because the absorption cross sections of N_2O were very small at these wavelengths, N_2O gas could not be used as a reference for $O(^1D)$ quantum yield determinations as done for the 193-nm experiments. The photolysis laser wavelengths were alternatively changed between each of the five wavelengths and 230 nm, while detecting the $O(^1D)$ atoms produced photolytically by the VUV-LIF technique. The probe laser wavelength was scanned over the $O(3s^1D^\circ - 2p^1D)$ transition line, which was broadened by Doppler effects due to the partitioning of the excess energy to the translational motion in the phtodissociation process of O_3. The $O(^1D)$ quantum yield at 230 nm has recently been reported to be 0.910 ($\pm$0.019) by Takahashi et al.,[9] which was used as a reference in the present study. Thus, the absolute quantum yield values at $\lambda = 206$, 210, 215, 220, and 225 nm were determined by the LIF intensity ratio measurements, using the following expression:

$$\Phi^{1D}{}_{O3}(\lambda) = \Phi^{1D}{}_{O3}(230) \times \frac{S_{O3}(\lambda)}{S_{O3}(230)} \frac{I(230)}{I(\lambda)} \frac{\sigma_{O3}(230)}{\sigma_{O3}(\lambda)} \qquad (5)$$

where $\Phi^{1D}{}_{O3}(230)$ is the $O(^1D)$ quantum yield at $\lambda = 230$ nm, $S_{O3}(\lambda)$ is the $O(^1D)$ LIF intensity from O_3 photolysis at the photolysis wavelength of λ, and $I(\lambda)$ is the photon flux of the UV photolysis laser. The cross-section values for O_3 absorption were taken from the report by Malicet et al.[4]

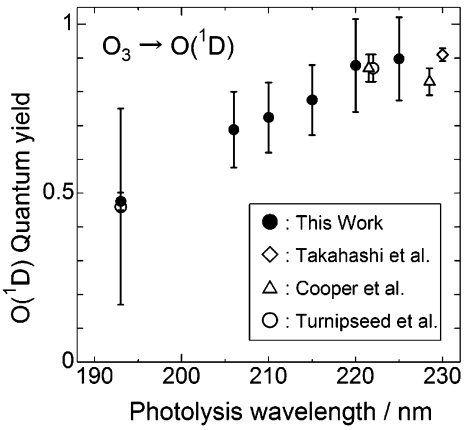

Figure 3. Quantum yields for $O(^1D)$ production in the photolysis of O_3 at 193, 206, 210, 215, 220 and 225 nm. The present results are indicated by filled circles, in which the error bars are 1σ statistical uncertainties (see text). For comparison, the former results by Takahashi et al.[9] (open rhombus), Turnipseed et al.[10] (open circle) and Cooper et al.[13] (open triangle), are also indicated.

Figure 3 shows the results of the present study to determine the $O(^1D)$ quantum yield from the photodissociation of O_3, $\Phi^{1D}{}_{O3}(\lambda)$, at photolysis wavelengths of $\lambda = 193$, 206, 210, 215, 220, and 225 nm at 298 $\pm$ 2 K, together with those of former studies by Turnipseed et al.[10](193 and 222 nm), Cooper et al.[13] (221 nm), and Takahashi et al.[9] (230 nm). Table 2 lists the quantum yield values of the $O(^1D)$ production from O_3 photolysis in the wavelength range of 193 and 225 nm. The quoted uncertainties of the presently determined values (Figure 3 and Table 2) include the statistical errors (1σ) of the LIF intensity measurements and the systematic errors estimated for the pressure and laser power measurements. For the LIF intensity ratio measurements, 5$-$20 sets of the experiments were performed at each photolysis wavelength.

At 193 nm, the $O(^1D)$ quantum yield obtained in this work is in excellent agreement with that reported by Turnipseed et al.[10] within the experimental uncertainties, as shown in Figure 3 and Table 2, while the quoted error for our result is significantly smaller than theirs. Stranges et al.[11] estimated the channel branchings for $O(^1D) + O_2(a^1\Delta_g)$ and $O(^1D) + O_2(b^1\Sigma_g^+)$ to be 0.455 $\pm$ 0.025 and 0.233 $\pm$ 0.020, respectively, for the $O(^1D)$ formation processes in the photolysis of O_3 at 193 nm. Their branching ratios were calculated from the analysis of the translational energy distribution of the oxygen atom fragments with a mass spectrometer, although their method could not detect the O atom fragments quantum-state selectively.

TABLE 2: Quantum Yields for O(^{1}D) Production in the Ultraviolet Photolysis of O_3 between 193 and 225 nm at 298 ± 2 K

	O(^{1}D) quantum yield	
λ,[a] nm	this work[b]	references
193	0.48 ± 0.03	0.46 ± 0.29[c]
206	0.69 ± 0.11	
210	0.72 ± 0.10	
215	0.78 ± 0.10	
220	0.88 ± 0.14	
221.5		0.87 ± 0.04[c]
222		0.87 ± 0.04[d]
225	0.90 ± 0.12	
228.5		0.83 ± 0.04[d]
230		0.910 ± 0.019[e]

[a] Photolysis wavelength of O_3. [b] Quantum yield values for O(^{1}D) production from O_3 photolysis, as determined in the present work. The quoted uncertainties include the statistical errors (1σ) of the LIF intensity measurements and the systematic errors estimated for the pressure and laser power measurements. [c] Reference 10. [d] Reference 13. [e] The O(^{1}D) quantum yield at 230 nm, which was reported by Takahashi et al.,[9] is used as a reference value to obtain the quantum yield values at 206−225 nm (see text).

The total of their branching ratios for the O(^{1}D) formation processes (0.688 ± 0.045) is larger than the values of $\Phi^{1D}_{O3}(193) = 0.48 \pm 0.03$ determined in this work and of $\Phi^{1D}_{O3}(193) = 0.46 \pm 0.29$ reported by Turnipseed et al.[10] The reason for the difference is not clear.

The present paper provides the first determination of the quantum yield values for O(^{1}D) production from O_3 photolysis in the wavelength range of 193 and 222 nm. Our results suggest that the O(^{1}D) quantum yield decreases monotonically as the photolysis wavelength becomes shorter from 220 to 193 nm. Above 198 nm, the sum of the quantum yields for O(^{3}P), O(^{1}D), and O(^{1}S) productions should be unity (Table 1). In our present study, we determined the O(^{1}D) quantum yield values at 206, 210, 215, 220, and 225 nm. A very recent study by Takahashi et al.[12] has revealed that the quantum yield for O(^{1}S) production is as small as 2.5 (±1.1) × 10^{-3} even at 193 nm. Therefore, the values of $1 - \Phi_{1D}(\lambda)$ above 198 nm should closely agree with the quantum yields for O(^{3}P) formation in the photodissociation reaction of O_3 between 198 and 234 nm, in which the wavelength of 234 nm is the thermochemical threshold for O(^{1}S) formation as listed in Table 1.

A decrease trend of the O(^{1}D) quantum yield from 220 to 193 nm is in contrast to the almost constant values of the quantum yield between 220 and 300 nm. This is attributable to the different dissociation dynamics of O_3 after photoexcitation at the blue side of the Hartley band and in the center of Hartley band. Many studies showed that the upper 1^1B_2 excited electronic state is responsible for the Hartley band transition.[2,19] In the wavelength region of 230−300 nm, about 91% of the photoexcited O_3 molecules dissociate directly to the O(^{1}D) + $O_2(a^1\Delta_g)$ products on the surface of the 1^1B_2 state, while the residual 9% switch their potential surface to the R state and dissociate to the O(^{3}P) + $O_2(X^3\Sigma^-_g)$ products.[1,2,9] Both the Doppler spectroscopy[14] and the photofragment translational spectroscopy[11] revealed that the fragment recoil anisotropy from the 193-nm photolysis of O_3 was different from that expected from the prompt dissociation from the 1^1B_2 state. At the blue side of the Hartley band, other mechanisms may account for the branching ratio for O(^{1}D)/O(^{3}P) productions in the photolysis of O_3 between 193 and 220 nm. One possible mechanism is that the O_3 molecules are photoexcited to an electronic state other than the 1^1B_2 state and dissociated preferably to the O(^{3}P) + $O_2(X^3\Sigma^-_g)$ products. Another possible mechanism is that a new electronic surface crossing can be reached above the photon energy of 230 nm on the 1^1B_2 surface and then O_3 molecules switch their surface through the new crossing and produce the O(^{3}P) + $O_2(X^3\Sigma^-_g)$ products preferably.

The latest NASA/JPL panel recommends the temperature-independent value of $\Phi^{1D}_{O3}(\lambda) = 0.90$ at $\lambda < 306$ nm and the short wavelength limit for the recommendation is not given exactly.[8] However, as shown in Figure 3, the present study indicates that the NASA/JPL recommendation is not valid in the range of 193−220 nm. For use of the O(^{1}D) quantum yield data in the atmospheric studies, we suggest a simple expression to derive the $\Phi^{1D}_{O3}(\lambda)$ values in the wavelength range of 193−225 nm as a function of photolysis wavelength λ:

$$\Phi^{1D}_{O3}(\lambda) = 1.37 \times 10^{-2} \times \lambda - 2.16 \quad (6)$$

This expression was obtained by linear least-squares fit analysis of the present experimental data of the O(^{1}D) quantum yield values.

We estimated the differences in the stratospheric O(^{1}D) production rates calculated with the constant value of $\Phi^{1D}_{O3}(\lambda) = 0.90$ (NASA/JPL recommendation) and with the wavelength-dependent $\Phi^{1D}_{O3}(\lambda)$ value given by eq 6. The O(^{1}D) production rate from O_3 photolysis is defined as follows:[20]

$$J^{1D} = \int \sigma_{O3}(\lambda)\Phi^{1D}_{O3}(\lambda)F(\lambda)\, d\lambda \quad (7)$$

In eq 7, $F(\lambda)$ is the altitude-dependent actinic flux. The partial J^{1D} values at $\lambda = 193-220$ nm account for 3.0, 4.6, and 2.2% of the total J^{1D} values in the whole wavelength region of 193−335 nm at 20, 30, and 40 km altitudes, respectively, in which the σ_{O3} values at 295 K reported by Molina and Molina[3] and the $F(\lambda)$ values at solar zenith angle (SZA) of 40°[21] are used. Thus, the total J^{1D} values estimated with eq 7 are smaller than those obtained with the NASA/JPL recommended constant value of $\Phi^{1D}_{O3}(\lambda) = 0.90$ by 0.7, 1.0, and 0.5% at 20, 30, and 40 km altitude, respectively.

It is interesting to refer to Houston and co-workers' work[22−24] related to the "ozone deficit" issue, which implicates the discrepancy between the modeled and observed O_3 abundance in the stratosphere. They suggested that the formation of the highly vibrationally excited $O_2(X^3\Sigma^-_g, v'' \geq 26)$ from the UV photolysis of O_3 could partly account for the ozone deficit issue through the possible reactive scattering of $O_2(X^3\Sigma^-_g, v'' \geq 26)$ by O_2:

$$O_3 + h\nu\ (\lambda \leq 243\ \text{nm}) \rightarrow O(^3P) + O_2(X^3\Sigma^-_g, v'' \geq 26) \quad (8)$$

$$O_2(X^3\Sigma^-_g, v'' \geq 26) + O_2(X^3\Sigma^-_g, v'' = 0) \rightarrow O_3(X^1A_1) + O(^3P) \quad (9)$$

$$2 \times \{O(^3P) + O_2(X^3\Sigma^-_g) + M \rightarrow O_3 + M\},\ M = N_2, O_2 \quad (10)$$

$$\text{Net: } 3O_2(X^3\Sigma^-_g) + h\nu \rightarrow 2O_3 \quad (11)$$

The formation of $O_2(X^3\Sigma^-_g, v'' \geq 26)$ in the UV photolysis of O_3 (reaction) has been reported by several groups.[22,23,25−27] Although no experimental evidence of the O_3 production in reaction 9 has been reported, the production efficiency of O_3 from reactions 8−11 in the stratosphere has been estimated.[22−24] Their estimation is based on the measured branching ratio between O(^{3}P) + $O_2(X^3\Sigma^-_g, v'' \geq 26)$ and O(^{3}P) + $O_2(X^3\Sigma^-_g, v'' < 26)$ and on assumption that the *total* quantum yield for

$O(^3P)$ production in the UV photolysis of O_3 is 0.1 between 193 and 243 nm. However, our present study clearly indicates that the $O(^3P)$ quantum yield ($=1 - \Phi^{1D}{}_{O3}(\lambda)$) in the $\lambda \leq 225$ nm region is larger than 0.1, as shown in Figure 3 and Table 2. Therefore, it is likely that the stratospheric O_3 production due to eqs 8−11 is more efficient than that estimated previously by Houston and co-workers.

Acknowledgment. The work was supported by Grants-in-Aid from the Ministry of Education, Culture, Sports, Science and Technology, Japan. The Sumitomo Foundation is also gratefully acknowledged for financial support.

References and Notes

(1) Matsumi, Y.; Comes, F. J.; Hancock, G.; Hofzumahaus, A.; Hynes, A. J.; Kawasaki, M.; Ravishankara, A. R. *J. Geophys. Res.* **2002**, *107*, 10.1029/2001JD000510.

(2) Matsumi Y.; Kawasaki, M. *Chem. Rev.* **2003**, *103*, 4767.

(3) Molina, L. T.; Molina, M. J. *J. Geophys. Res.* **1986**, *91*, 14501.

(4) Malicet, J.; Daumont, D.; Charbonnier, J.; Parisse, C.; Chakir, A.; Brion, J. *J. Atmos. Chem.* **1995**, *21*, 263.

(5) Voigt, S.; Orphal, J.; Bogumil, K.; Burrows, J. P. *J. Photochem. Photobiol.* **2001**, *A143*, 1.

(6) Atkinson, R.; Baulch, D. L.; Cox, R. A.; Hampson, R. F., Jr.; Kerr, J. A.; Rossi, M. J.; Troe, J. *J. Phys. Chem. Ref. Data* **1997**, *27*, 1329.

(7) Ravishankara, A. R.; Hancock, G.; Kawasaki, M.; Matsumi, Y. *Science* **1998**, *280*, 60.

(8) Sander, S. P.; Friedl, R. R.; Golden, D. M.; Kurylo, M. J.; Huie, R. E.; Orkin, V. L.; Moortgat, G. K.; Ravishankara, A. R.; Kolb, C. E.; Molina, M. J.; Finlayson-Pitts, B. J. *Chemical Kinetics and Photochemical Data for Atmospheric Studies*, JPL Publication 02-25, JPL, Pasadena, CA, 2003.

(9) Takahashi, K.; Hayashi, S.; Matsumi, Y.; Taniguchi, N.; Hayashida, S. *J. Geophys. Res.* **2002**, *107*, 10.1029/2001JD002048.

(10) Turnipseed, A. A.; Vaghjiani, G. L.; Gierczak, T.; Thompson, J. E.; Ravishankara, A. R. *J. Chem. Phys.* **1991**, *95*, 3244.

(11) Stranges, D.; Yang, X.; Chesko, J. D.; Suits, A. G. *J. Chem. Phys.* **1995**, *102*, 6067.

(12) Takahashi, K.; Nakayama, T.; Matsumi, Y. *J. Phys. Chem. A* **2003**, *107*, 9368.

(13) Cooper, I. A.; Neill, P. J.; Wiesenfeld, J. R. *J. Geophys. Res.* **1993**, *98*, 12795.

(14) Takahashi, K.; Matsumi, Y.; Kawasaki, M. *J. Phys. Chem.* **1996**, *100*, 4084.

(15) Hilbig R.; Wallenstein, R. *Appl. Opt*. **1982**, *21*, 913.

(16) Heidner, R. F., III; Husain, D. *Int. J. Chem. Kinet.* **1974**, *6*, 77.

(17) Nakayama, T.; Takahashi, K.; Matsumi, Y.; Taniguchi, N.; Hayashida, S. *J. Geophys. Res.* **2003**, *108*, 10.1029/2003JD003709.

(18) Nishida, S.; Takahashi, K.; Matsumi, Y., Taniguchi, N.; Hayashida, S. *J. Phys. Chem. A.* in press.

(19) Hay, P. J.; Pack, R. T.; Walker, R. B.; Heller, E. J. *J. Phys. Chem.* **1982**, *86*, 862.

(20) Brasseur, G. P.; Orlando, J. J.; Tyndall, G. S. *Atmospheric Chemistry and Global Change*; Oxford University Press: New York, 1999.

(21) Kylling, A.; Stamnes, K.; Tsay, S.-C. *J. Atmos. Chem.* **1995**, *21*, 115.

(22) Miller, R. L.; Suits, A. G.; Houston, P. L.; Toumi, R.; Mack, J. A.; Wodtke, A. M. *Science* **1994**, *265*, 1831.

(23) Geiser, J. D.; Dylewski, S. M.; Mueller, J. A.; Wilson, R. J.; Toumi, R.; Houston, P. L. *J. Chem. Phys.* **2000**, *112*, 1279.

(24) Houston, P. L.; Suits, A. G.; Toumi, R. *J. Geophys. Res.* **1996**, *101*, 18829.

(25) Syage, J. A. *J. Chem. Phys.* **1996**, *105*, 1007.

(26) Kinugawa, T.; Sato, T.; Arikawa, T.; Matsumi, Y.; Kawasaki, M. *J. Chem. Phys.* **1990**, *93*, 3289.

(27) Takahashi, K.; Taniguchi, N.; Matsumi, Y.; Kawasaki, M. *Chem. Phys.* **1998**, *231*, 171.